AIRBORNE SPECTRORADIOMETER ANALYSIS AND LANDSAT MAPPING OF HYDROTHERMAL ALTERATION

William Collins

NASA, Institute for Space Studies
Goddard Space Flight Center
New York, N. Y. 10025

and

Columbia University, New York, New York

CONTENTS

AIRBORNE SPECTRORADIOMETER ANALYSIS AND LANDSAT MAPPING OF HYDROTHERMAL ALTERATION

By

William Collins

NASA, Institute for Space Studies
Goddard Space Flight Center
New York, N. Y. 10025

and

Columbia University, New York, New York

Abstract

An airborne spectroradiometer system has been developed to take simultaneous 500 channel ground target measurements in the spectral region between 400 nm and 1100 nm. Survey flights with the instrument over an exposed hydrothermal alteration zone in Goldfield, Nevada provide the high spectral resolution and spatially correlated data necessary to establish a computerized technique for spectral discrimination of limonitic zones that could indicate mineralization. The data generated by the airborne system is used, in particular, to determine the spectral properties of alteration materials as they appear in integrated measurements over extended field areas, to determine

which spectral properties are unique under field conditions and will remain unique in the low spectral resolution LANDSAT data, and to accurately determine the nature and magnitude of the relative spectral differences among geologic targets under the broad band configuration.

Field measurements from the aircraft are spatially integrated over contiguous 18 meter square fields of view along traverses flowing to cover both background and altered rock assemblages. A small spectral signal unique to zones enriched in ferric iron minerals is recoverable in the aircraft data. Based on a differential spectral discriminant, a computer-compatible method has been devised to extract the ferric iron signal from atmospheric and geologic "noise" in LANDSAT data.

The discrimination technique, adapted to satellite spectral data, was applied to the Goldfield, Nevada region, including the area of known alteration and metallic mineralization. Field reconnaissance and comparison with published maps for this region has affirmed that limonitic alteration is accurately delineated by the computer analysis technique.

INTRODUCTION

Computer produced maps of exposed hydrothermal alteration in the Goldfield, Nevada district have been obtained using a combination of airborne spectral data and specialized techniques of LANDSAT data analysis. The visible and near infrared spectral properties of altered rock and surface coatings of limonitic minerals were determined under field conditions with the aid of a custom designed airborne spectro-radiometer system. The aircraft data is especially crucial in determining the spectral characteristics of extended, heterogeneous targets in their natural geologic settings, as they appear to broad band pass and spatially integrating remote radiometer sensors. The lack of this basic information has, to a large extent, hindered past efforts to develop the full potential of the LANDSAT broad band multi-spectral system as a tool of mineralogical exploration.

Satellite discrimination of limonitic alteration has been proven possible by Rowan, et al. (1974). Altered areas appear as tonal anomalies in their color composite images produced from computer ratioed and contrast-stretched LANDSAT spectral data of the Goldfield, Nevada area. It has not been possible, however, to extract from the LANDSAT data alone sufficient quantitative information to permit satisfactory computerized analysis and discrimination of altered rock. The spectral signals of altered rock, under the low wavelength and spatial resolution of the satellite instrument, are very subtle and are overwhelmed by larger "noise" variations in the data. Laboratory measurements (Hunt, et al., 1971) and ground field measurements (Goetz, et al., 1975; Rowan, et al., 1977) have been made on the alteration materials and the limonitic weathering products, but these measurements cannot be extrapolated to the remote,

spatially integrating sensors used in airborne or orbiting surveys. To bridge the gap between present knowledge of the spectral properties of materials and the properties of extended targets observed by remote spectral sensors, the Goldfield district was flown with the airborne spectroradiometer system. Survey sites were selected with much appreciated field assistance from Larry Rowan and Roger Ashley of the U.S. Geological Survey and from their published work on the area (Rowan, et al., 1974; Ashley, 1971; 1974).

The airborne system includes a parallel input, rapid spectral-scanning device with 500 channels of spectral data at 1.4 nm wavelength intervals. Spectral measurements of the Goldfield area were integrated over 18 meter square target areas containing all of the major classes of materials in the region including background rock and altered outcrop. These aircraft data are computer analyzed to establish, in particular, the degree to which spectral features of alteration zone rocks and minerals, as they are known from laboratory measurements, still persist and are unique under field conditions of hetergeneous targets, low spatial resolution, varying spectral resolution (simulated broad bands), and radiation field and geologic noise. A method for discriminating limonitic alteration zones under field conditions has been derived from the aircraft data analysis and adapted to satellite data and a computer classification algorithm. Resulting spectral discrimination maps of the Goldfield region, produced in the computer using LANDSAT data, accurately delineate alteration zones in the Goldfield region.

Nature of Remote Radiance Measurements

Satellite and other remote spectral radiance measurments contain a substantial amount of inherent uncertainty introduced by the usually incalculable effects of spatial integration over heterogeneous targets in an extended field of view, and by the effects of other numerous ground target and radiation field variables. In general functional form, the apparent spectral radiance at the entrance aperture of a remote radiometer viewing an extended target can be expressed

$$N_{\lambda_{sensor}} = N_{\lambda_{target}} [\tau_a ; \lambda ; x,y ; \Delta x, \Delta y ; \rho' (\theta_i , \phi_i ; \theta_r , \phi_r) ; t] + N_{\lambda_{path}}$$

$$[w \cdot cm^{-2} \cdot sr^{-1} \cdot \mu^{-1}] . \qquad (1)$$

The radiance term $N_{\lambda_{target}}$ is the reflected spectral radiance, which includes energy incident directly from the sun plus energy from the atmosphere and adjacent ground areas scattered onto the target. The terms x, y and Δx, Δy are the ground location and field of view -- the kinds and amount of materials under observation and their proportions and distributions. The bidirectional reflectance properties of the target materials ρ' include the elevation and azimuth angular dependencies with respect to incident radiation θ_i, ϕ_i and to the measurement direction of reflected radiation θ_r, ϕ_r. Time dependency t includes solar angle and seasonal effects. The atmospheric effects include the multiplicative transmittance factor τ_a and the additive path radiance factor $N_{\lambda_{path}}$. All factors are wavelength λ dependent.

Spectral information is especially difficult to extract from satellite measurements in geologic applications because of the very small range in variation among the spectral data of rocks and soils and because of the typically wide range in variation of rock-soil-vegetation mixtures over a satellite field of view. In most cases, the discriminating spectral signals occurring over alteration are submerged among much larger signals contributed by a combination of other target and radiation field variables, including non-spectral albedo variations. LANDSAT data from 4779 targets in a 4 kilometer square area encompassing Goldfield are shown in Figure 1, where the four spectral band measurements for each target have been transformed into spectral vectors in four dimensional hyperspace. The six principal plane projections of the

Figure 1 near here

4779 vectors are shown in the plots. The vector projections form tight, uniform clusters of points stretched along the vector length direction. The stretch along vectors, which pass approximately through the origin, is due to albedo variations among targets. By far the greatest signal variation is in the albedo, or magnitude of the spectral vectors. Spectral differences are indicated in the vector slope variations, which are very small. Superimposed on the small spectral variations due to rock type are those due to vegetation, shadows, ground slope and texture, and other variables in the target area (all of which contribute to the geologic noise), plus the variations due to the radiation field noise.

Computerized discrimination using cluster analysis methods has not proven very successful for separating rock types because of the tight and more or less uniform clustering of the rock spectra. The targets form only one spectral cluster and any preferred distribution of points within the cluster is usually more pronounced in the albedo direction. The discrimination method used in the present investigation avoids the use of a cluster or statistical distribution criterion; instead it relies on predetermined

criteria of vector analysis based on a specific and predictable variation of spectral vectors within the general group of rock vectors. In using a differential spectral signal, the effects of most radiation field and instrument factors are minimized. The discrimination method also circumvents the need for recognition of specific target "signatures", which change in an unpredictable way with changes in radiation field and instrument characteristics.

ACKNOWLEDGEMENTS

This study was supported by a research grant to Columbia University from the National Aeronautics and Space Administration, Goddard Institute for Space Studies. Laboratory and computer support was provided at the facilities and by the personnel of the Institute for Space Studies (GISS). The research was made possible by Dr. Robert Jastrow, director of GISS, through his generous personal support and advice; by Prof. Peter Ypma, University of Adelaide, who established the remote sensing project at Columbia University; by Dr. Stephen Ungar, GISS, who designed and supervised much of the computer programming support required for the aircraft and satellite data processing; and by Dr. Hong-Yee Chiu, GISS, who designed and helped to build the logic circuitry in the instrument interface. Invaluable aid was extended by Larry Rowan and Roger Ashley of the U.S. Geological Survey. I am grateful to them for the fruitful discussions and their assistance in setting up the airborne survey and field work in Goldfield.

GEOLOGY OF THE REGION

The Goldfield mining district lies on the eastern edge of Esmeralda and adjacent parts of Nye counties in west central Nevada, among a group of low rolling hills. Elevation ranges from 1680 meters on the western side of the district to 2100 meters in the hills to the East. The hills below 2150 meters and the pediments are covered with 10 to 30 percent desert vegetation, mostly sagebrush, while the higher ranges support heavier growth of piñon pine and junipers. Rock outcrops are exposed on hills and ridges, intervening valleys are covered with pediment gravels and alluvium.

Gold and silver were mined in the earlier part of this century from epithermal deposits in Tertiary volcanic rocks. The Goldfield district is one of many similar Tertiary volcanic centers found in the basin and range province (Albers and Kleinhampl, 1970). Alteration and ore deposition typically took place along fault controlled zones in andesitic and rhyolitic units deposited during the earlier phase of volcanic activity. Erosion has exposed the altered zones leaving the highly silicified cores standing as ridges with the outer argillic zones exposed along the ridge flanks.

Quartz monzonite basement rock in the center of the district is surrounded by a concentric pattern of older to younger Tertiary volcanic rock units going outward (Figure 2). The dissected dome structure indicates a resurgent magma chamber centered roughly under the district (Albers and Kleinhampl, 1970). The action of caldera collapse during extrusive periods and doming during resurgency generated an elliptical pattern of many small steep angle faults (Ashley, 1974). A fracture zone also extends southeast from Blackcap Mountain. The fracture pattern has been mapped in detail by Ashley (1971) but, in order to preserve the geologic relations, is

Figure 2 near here

not included on the adaptation of his map. Hydrothermal fluids in the last stage of the volcanic cycle followed along the fracture system leaving the pattern of alteration shown on the map.

Hydrothermal alteration along the fault controlled zones produced classic zonation in the altered host rock. The rock in vein core zones is leached and replaced by colloidal silica, alunite, pyrophyllite, and kaolinite. The adjacent argillic alteration includes an illite-kaolinite zone near the core and an outer montmorillonite zone (Harvey and Vitaliano, 1964). The exposed silicified ledges are coated with dark botryoidal crusts of hematite and goethite. Jarosite, hematite, and goethite mineralization and staining color the outcrop and argillic rock and soil various hues of yellow, brown, red and purple.

AIRCRAFT DATA ANALYSIS

The airborne spectroradiometer system assembled for this study is designed to take high wavelength resolution spectra in rapid sequence from a low-flying, light aircraft (Collins, 1976; Chiu and Collins, 1977). The system takes 500 spectral band measurements in 1.4 nm wide increments between 400 nm and 1100 nm. The parallel input electro-optical design of the system (Princeton Applied Research Corp. 1975) allows rapid sensor read-out, 30 spectra per second at 500 bands per spectrum, with high sensitivity and optimum ground registration from band to band. The system is flown at 610 meters altitude; spectral measurements are integrated over 18m square fields of view in a one dimensional sequence along the flight path. The data comes out of the system in digital form and is stored on computer-compatable type.

Analysis of the airborne survey data takes advantage of the several kinds of information available in the spectral data and coincident flight film, which, in combination, make this airborne technique uniquely different from ground and satellite spectral measurements. The rapidly acquired and contiguous spectral measurements, along flight lines planned to cross both background and altered zones, are computer processed to compare the relative variations in selected spectral regions sensitive to ferric iron absorption. Using the simultaneously acquired aerial photographs, the spectral variations are correlated with geologic ground truth. Selected spectral curves along the flight line are compared with laboratory spectra at high wave length resolution to establish how the known spectral features of alteration products (mainly the limonitic minerals) appear in field measurements, which under survey conditions are spatially integrated over varying mixtures of naturally occurring materials in a target area. The relative spectral variations among background targets indicate the normal exposed terrain variation, or

geologic noise. The spectral difference between background and altered rock, once proven unique to ferric iron mineralization and greater than background noise, can be exploited in computer discrimination and mapping schemes, which, however, must be specialized to fit the wavelength and spatial resolution of the particular survey instrument.

Choice of Bands for Data Reduction and Analysis

The large volume of field data on tape is analyzed initially by reducing the 500 channel data to a small number of discrete bands which are examined by ratio techniques. The choice of bands for ratioing is based on laboratory spectra of whole rock samples taken from outcrop within the airborne survey region. Spectral measurements are made on the weathered surfaces using the same 500 channel spectroradiometer employed in the airborne operations. Four reflectance spectra of rock samples rich in ferric iron minerals are shown in Figure 3. The rock sample spectra are corrected for instrument spectral response and light source characteristics by ratioing with the spectrum of a white reflectance standard, but they are not corrected for irradiation differences due to surface roughness and orientation of the samples. The spectra of

---

Figure 3 near here

---

hematite, limonite (the hydrated ferric iron minerals), and jarosite have a strong blue-green absorption edge typical of the ferric ion (Hunt and Salisbury, 1970). A weaker absorption region extends from the shoulder at 600 nm to the peak at 750 nm. Ferric iron absorption in the infrared is well developed in a broad band centered at about 900 nm. The position of the infrared absorption minimum shifts toward the longer wavelengths in the limonite and jarosite spectra. The minimum for jarosite is 50 nm farther into the infrared than the minimum for hematite. The shape and

location of the absorption edge in the visible region also varies according to the mineralogical state of the ferric ion. The relative variation in the visible and infrared absorptions causes the apparent peak in the red region to shift between 700 nm and 750 nm. These small but distinguishing variations in the spectral curves of ferric iron minerals are potentially useful for differentiating alteration zones from hematite rich sedimentary and volcanic rocks with the use of high spectral-resolution survey instruments.

For analysis of wide band variations in rock spectra, 50 nm wide bands were selected in the two ferric iron absorption regions and at the intervening peak, or area of least absorption. These bands are centered at 500 nm, 750 nm and 900 nm in Figure 3. Another band centered at 660 nm, the chlorophyll absorption region, was selected to allow separation of target areas with heavier vegetation. The wide band measurements are simulated from the high spectral-resolution aircraft data along each flight line by integrating the radiance over the four selected portions of the spectral curves. The combinations of band ratios have been plotted with respect to the ground track in Figures 4 and 5. The bands ratioed are labelled 1, 2, 3 and 4 corresponding to the bands centered at 500 nm, 660 nm, 750 nm, and 900 nm respectively.

Aircraft Traverses

The ratios of bands, 1, 2, and 3 for 350 spectra taken along survey flight line 24 are plotted with respect to position along the flight line in Figure 4. The ground

Figure 4 near here

track of the flight line, flown east to west, is plotted on the geologic map in Figure 2. Rock unit boundaries and the alteration limits shown on the ratio plots are taken from

the geologic map. The flight line traverses the two most intensely altered and mineralized Tertiary host rock units in the Goldfield complex, rhyodacite and Milltown andesite. The traverse begins in unaltered rock and passes into altered rock of the same units. No unique spectral difference among unaltered rock units appears in these band ratios; however, a significant difference in band 1 ratios does appear in the data from the altered zone as compared with unaltered areas. The greater concentration of limonitic minerals, oxidation products of sulfides in the altered and enriched zone, is indicated by the increased absorption in band 1.

The 2/1 band ratios of background rock and alluvium in the first 150 spectra of the flight line vary between 1.00 and 1.25 (Figure 4). Band 3/1 ratios show greater variation, and the mean ratio values are lower. The 2/1 and 3/1 band ratios increase up to 30 per cent above the background signals over the alteration zone while the 3/2 band ratios remain fairly constant. The increase above 1.25 in band 1 ratios at spectrum 40 and between spectra 120 and 140 occurs where the flight line runs near the edge of the alteration zone, as shown on the geologic map. Ratio values greater than 1.00 in the 3/2 band combination, and 3/1 band ratios greater than the 2/1 values, are noise effects produced by vegetation cover in the target areas. The aerial photos show that the high 3/2 and 3/1 band ratios occur along the flight line where alluvial washes support heavier desert vegetation.

The maximum spectral signal indicating ferric iron minerals occurs on the western edge of the Goldfield district. Flight line 2 of Figure 5 shows a 60 percent increase above background in the 2/1 and 3/1 ratios between spectra 75 and 85.

Figure 5 near here

This high signal appears over a zone of post-alteration Siebert Tuff that contains a several hundred foot thick fanglomerate bed of hydrothermally altered material from the altered zone to the north. Well exposed landslide debris containing porphyritic rhyodacite and Milltown andesite clasts are stained and cemented by abundant limonitic minerals (Ashley, 1974). The Siebert Tuff in the earlier part of the flight line, spectra 1 through 60, has only background concentrations of ferric iron. Mine dump tailings in flight line 2 are indicated by low 3/2 and 3/1 ratios, which distinguishes them from other rock and alluvium.

Discriminating Bands

Aircraft spectra of selected targets in flight line 2 are plotted in Figure 6. The ferric iron absorption band in the blue-green visible region is very prominent in the

Figure 6 near here

limonitic Siebert Tuff spectra as compared with the other two spectra of unaltered tuffaceous rock from the Siebert Formation. The shape of the ferric iron absorption edge in the visible region, compared with the laboratory spectra of Figure 3 indicates hydrated ferric iron minerals. The sharp break upward in the absorption edge at 530 nm and the shoulder at 600 nm is characteristic of the limonitic spectrum in Figure 3 and different from both the jarosite spectrum, which does not have the well-developed absorption edge, and the hematite spectrum, which breaks upward at 570 nm with the shoulder at 615 nm. That the location and shape of the blue-green absorption edge appears so distinctly in the field spectra strongly supports further use of high resolution airborne spectroradiometry for separating the hematitic areas from altered zones high in ferric iron hydrates and sulfates.

The near IR absorption band appears weak and variable in the field spectra of limonitic targets in Figure 6. The band 4/3 and the 4/2 ratios should be sensitive to

ferric iron absorption in the 900 nm IR spectral region (Band 4). These ratios, however, show only a slight change, decrease, in the heavily limonitic section of flight line 2 (Figure 5). They drop more distinctly below the background mean and extreme of variation in some other less limonitic parts of the altered zone. The Band 4 variations, then, do not appear to follow the limonite related variations in the band 2/1 and 3/1 ratios along the flight line. A spectrum of a target area with low 4/2 and 4/3 ratios (mine tailings) is plotted in Figure 6. The slope of the blue-green absorption edge and the deeper absorption in the 900 nm region are similar to the spectral features of jarosite in Figure 3.

The aircraft data suggest that jarosite in an alteration area could have a significant effect on the near IR region. In the present aircraft data and ground truth, however, there is not enough information to explain the observed variations and the possible influence of vegetation in this spectral region. The spectral data in the first three bands, on the other hand, clearly show variations as high as 60 percent above background occurring in the band 1 ratios over the limonitic zone. This variation is unique to the ferric iron minerals and cannot be confused with the effects of vegetation which change the 3/2 and 3/1 band relationships.

Spectral Signal Contrast

The 60 percent range in flight line 2 ratios indicates the upper limit of the ferric iron signal, which was obtained under near optimum conditions of spectral band width and position and with high ferric iron mineralization over a large uniform zone. The more common occurrence of lower and unevenly distributed concentrations of the limonitic minerals over a field of view, with still optimized band configuration, is indicated in the flight line 24 ratios (Figure 4). The maximum signal there is 30

percent above background, and most signals are considerably below that -- about 15 percent above background. The implication in flight line 24, that the discriminating spectral signals are small under most field conditions, holds true in the other flight lines shown on the map (Figure 2) but not presented.

The aircraft data show how altered zones differ using the selected narrow bands in optimum spectral positions. Under the LANDSAT wide-band configuration, the ferric iron spectral signals are still detectable but the contrast is greatly reduced. The three LANDSAT bands used for ferric iron discrimination in this study are approximately 100 nm wide and centered at 550 nm, 650 nm, and 750 nm. These bands have been simulated in the aircraft data from the flight lines shown in Figures 4 and 5. The LANDSAT spectral responsivity functions for each band (Hughes Aircraft Co., 1972) were folded into the simulation. Under the simulated satellite spectral responsivity, the band ratio curves along the flight lines retain the same general shape and still contain most of the same information found under the optimum band configuration (Collins, 1976). There is, however, a 50 percent decrease in contrast between background and ferric iron rich targets. The degradation in contrast seriously effects the alteration signal bringing the average ratio variations over the altered zone down to less than 10 percent above background.

ROCK DISCRIMINATION AND MAPPING USING LANDSAT DATA

For analysis and discrimination using large volumes of data, the spectral data and the ratio information are transformed into the color vector space domain. In color space, the ground spatial relationships are temporarily lost, but spectral differences are easily interpreted as variations in vector direction. The vector difference between areas of background and limonitic rock, determined from the simulated LANDSAT data, are used to establish the discrimination parameters to be applied in a color space model for detecting very small variations in spectral signals. This model is designed, in particular, to make precise spectral separation of ferric iron vectors within the tightly grouped vectors of all general catagories of rock and alluvium targets. Based on ground testing areas for which the spectral characteristics of the background and limonitic rocks are known from the airborne surveys, the model parameters can be emperically adjusted to fit the real LANDSAT data. The color space model has been adapted to LANDSAT data using a "Color Vector Classification Algorithm" (Ungar, 1976) developed at Goddard Institute for Space Studies.

Color Space Model

In color space, the three band ratios are the slopes of the unit vector projection onto the corresponding principle planes of the three dimensional coordinate system. The average of the ratio values in each of the three ratio combinations from background areas (e.g. first 150 spectra of flight line 24, Figure 4) can be translated into a single mean background vector function in the color space domain. Background rock and alluvium are represented by the resultant mean vector function $\bar{R}$ in three dimensional color

Figure 7 near here

space of Figure 7. The individual spectral vectors from background areas of exposed geology cluster tightly about the mean vector function. Individual vector lengths vary

along the mean vector function as a multiplicative factor of the absolute radiances in the three spectral bands (albedo function).

The ratio variation limits for background noise describe the vector direction tolerance (or color variation limits) in the color space model. The geologic noise variation (spectral component) in the 3/2 ratios of the simulated LANDSAT data translate into a ±3 degree maximum vector direction variation on the B3/B2 principle plane. The small 3/2 ratio variation among rock spectra, $\Delta \bar{R}_2$ and $\Delta \bar{R}_3$ in the color space domain, establishes fine limits into which color vectors must fall to be classified as rock or alluvium of any kind. Spectral vectors corresponding, for example, to ground areas high in vegetation will fall out of the rock catagory limits, toward B_2, due to chlorophyll absorption in band 2.

The surface concentration of ferric iron minerals in a target area is measured by the magnetude of the difference vector $\Delta \bar{R}_\perp$ in the direction perpendicular to the curved plane β, $\Delta \bar{R}_3$, $\Delta \bar{R}_2$. The plane curvature along the vector function $\bar{R}$, which intercepts the B2/B1 plane at β, is caused by additive atmospheric effects ($N_{\lambda_{path}}$ in Equ. 1). Vector variation in the approximate direction of the B_1 axis $\Delta \bar{R}_\perp$ is induced by ferric iron absorption in the blue-green visible region of the spectrum. The background geologic noise variation along the difference vector $\Delta \bar{R}_\perp$ is 3 degrees in the aircraft data under simulated LANDSAT spectral resolution. Spectral vectors from the altered areas vary up to 12 degrees in the $\Delta \bar{R}_\perp$ direction.

Adapting the Simulation Model to Satellite Data

The vector variation parameters in the model are derived from the spectral variation in aircraft data that has been calibrated to LANDSAT instrument spectral

responsivity in the simulation. These relative values should be close to those for the real LANDSAT data except for the differential spectral effects of radiation field variables (noise), and the effects of the larger satellite field of view. The vector space relationships will be effected by spatial variations in the optical density of the atmosphere over the survey region and by atmospheric changes over the measurement period (τ_a and $N_{\lambda_{path}}$ in Equ. 2). Spectral changes due to the bidirectional reflectance properties of target materials for solar positions at the time of the satellite measurement vs. the aircraft measurement ($\rho'(\theta_i, \phi_i; \theta_r, \phi_r)$) could also effect the color space relationships. During both the satellite and the aircraft missions, the sky was clear of visible clouds, and the ground visibility was 40 miles or more. Data from both missions were taken over a short time period and at similar sun angles. The effects of these indeterminate field variables were thus minimized.

Material distribution in the 20 times larger satellite field of view will introduce a difference in the magnetude of the relative spectral responses of the two instruments in most terrains. Limonitic outcrop less than 80 meters across (LANDSAT field of view) and situated in a background area of non-limonitic rock and soil will produce an attenuated spectral signal of ferric iron absorption when viewed by the satellite instrument. This problem can be avoided partly by adapting the model in carefully selected training areas. Because the aircraft instrument integrates radiance over an 18 meter square ground area, spatial information over ground elements on that order of size is preserved in the ratio plots. In certain sections along the flight lines, band 1 ratio peaks span twenty or more consecutive aircraft fields of view indicating broad ground areas where the satellite field of view would be most uniformly filled by ferric iron rich material. Integration by the LANDSAT sensor over ground areas with higher frequency variations in the ratio peaks would more likely result in the subdued spectral signals of

ferric iron minerals. The magnitude of spectral variation among rock spectra, as determined from aircraft data, is best applied to the satellite data in ground testing areas showing the broadest ratio peaks.

The direction of the mean vector function $\bar{R}_s$ for satellite data from background terrain will be shifted relative to the mean vector function $\bar{R}_a$ for aircraft data by a constant component that will not effect the discrimination parameters. The radiance in a LANDSAT band R_s received at the front aperture of the satellite can be related to the radiance in the same band R_a received at the aircraft aperture by $R_s = \alpha R_a + \beta$, where α and β are the absorption coefficient and path radiance of the atmospheric path between the aircraft and the satellite. The constant components of spectral vector shift considered here are due to the increased optical path through an atmosphere horizontally uniform across the survey region. The measured radiances R_s and R_a are also effected by a constant error factor in the absolute radiance calibrations of the two systems and by the difference in solar irradiance angle at the two survey times. The group of rock vectors and $\bar{R}_s$ shift position in color space, but the vector interrelations $\Delta \bar{R}_2$, $\Delta \bar{R}_3$, and $\Delta \bar{R}_\perp$ within the group, which are due to target spectral properties, are not significantly affected by these constant factors.

Only the direction of the mean background vector function $\bar{R}_s$, then, requires adjustment for a good first approximation fit to the satellite data. The direction and magnitude relationships among the limiting vectors $\Delta \bar{R}_2$ and $\Delta \bar{R}_3$ and the difference vector $\Delta \bar{R}_\perp$ are retained from the model. The adjustments to fit the model to the data are tested on ground areas of background, limonitic, and very heavily limonitic targets chosen from the spectral and spatial distribution information in the aircraft data. After fitting the mean background vector function $\bar{R}_s$ to the new data, increments in magnitude of variation along the difference vector $\Delta \bar{R}_\perp$ are selected empirically for best

separation of the background and two grades of limonitic test targets. An of the advantage of the color space model is that the direction of the difference vector remains constant (it is a function of the spectral position of the ferric iron absorption band); but the magnitude of the difference vector can be incremented to fit the application, the terrain spectral properties, and the noise factors.

Mapping with LANDSAT Data

Mapping with LANDSAT data using the adjusted discrimination parameters has been applied to a 25 kilometer square region centered on the Goldfield test area (Figure 8). Background vectors are incremented along the vector length to give 10 background levels of total brightness in the three spectral bands (albedo contrast). This albedo subdivision is displayed as a grey scale pattern by chosing computer printer symbols

---

Figure 8 near here

---

according to the print density. Background areas of basalt caps appear dark on the printout, and dry washes appear light. The grey scale is used for orientation.

Printer symbols indicating spectrally distinguished areas with ferric iron rich targets have been outlined for spectral contrast in the presentation of Figure 8. Alteration and sulfide enrichment in the Goldfield District is believed to have occurred along a large ring fracture zone above a collapsing magma chamber. Fracturing and alteration was more active on the southern rim and along an extended fracture zone to the southeast (Ashley, 1974). The southern part of the alteration zone pattern is well reproduced in the satellite spectral discrimination map. The ring fracture appears as a circular zone about 13 kilometers across in the center of Figure 8.

The ferric iron zone mapped 8 kilometers north east of the alteration ring, is a hydrothermally altered vent with limonitic staining but no significant heavy metal enrichment (R. P. Ashley, personal communication). The large area detected just to the west of Malpais Mesa (western edge of Figure 8) is the site of the Nevada Eagle Mine and several other prospects. This is a region of low silver production in heavily limonitic airfall tuff and tuff breccia of rhyolitic composition, which is synchronous with the Siebert Tuff unit. The extent of hydrothermal alteration and its relation to metal enrichment has not been studied. Zones high in ferric iron minerals appear 13 kilometers east of the Goldfield ring fracture and 16 and 29 kilometers northeast. These are areas of near surface hydrothermal alteration and limonitic mineralization, but apparently with no significant heavy metal enrichment (R. P. Ashley, personal communication).

ANALYSIS

The corrections required in adapting the discrimination model to the real LANDSAT data are due mainly to the effects of the atmosphere, the larger field of view, and systems calibration errors. These contributing effects cannot be deconvolved from the overall correction factors. But assuming that the relative calibration errors are small, the spectral changes indicated by the shifted mean vector function $\bar{R}_s$, and by a decrease in the maximum difference vector $\Delta \bar{R}_\perp$ for ferric iron targets, are consistent with the expected effects of increasing the atmospheric path length, and of increasing the sensor field of view. The greater atmospheric path length for satellite received radiation causes the mean background vector function to shift toward the B_1 axis and away from the B_3 axis indicating greater path radiance β at the shorter wavelength end of the spectrum and greater absorption α at longer wavelengths. These constant components of atmospheric effect on the spectral signals do not alter the inter-vector discrimination parameters. The larger size of the satellite field of view, however, causes degradation in the discriminability by decreasing the vector difference $\Delta \bar{R}_\perp$ of limonitic targets by an average of 1.0 degree. This amounts to an additional 15 percent loss in spectral contrast due to the satellite system configuration.

The field of view induced variation in spectral contrast is an independent function of the distribution of materials in the spectroradiometer field of view. As such, it is a systematic source of error added to the "geologic noise". The field of view phenomenon will cause heavily limonitic outcrop in a low ferric iron background setting in one field of view to appear spectrally similar to broadly uniform areas with only moderate amounts of ferric iron minerals. This effect results in some uncertainty in the interpretation of ferric iron signals. For example, playas and pediments with only

moderate concentrations of ferric iron minerals, but with broad, uniform exposure, appear more heavily mineralized in the LANDSAT measurements because of the relatively large total effect of ferric iron absorption over the integrated field of view. These areas, however, can be identified as playas and pediments by their morphology in the LANDSAT imagery.

In addition to the constant component of atmospheric effect on spectral signals, there is a variable noise factor due to wavelength dependent variations in α and β across the LANDSAT survey region. These lateral variations in the atmosphere introduce atmospheric noise that is in addition to the 3 degree geologic noise and the 1 degree uncertainty caused by the field of view phenomenon. Band to band variations in α and β for separate satellite passes over Goldfield determined empirically in an analysis by Kiang and Collins (1976) and compared to atmospheric study models (Hansen, 1969) in that analysis. The empirical study indicates a ±1 degree atmospheric noise effect on the vector direction in the worst case. The models indicate less atmospheric noise variation in vector direction for visibility changes from 24 to 112 kilometers in a theoretical atmosphere. Considering the worst case of ±1 degree, the atmospheric noise will not prevent discrimination of significant limonitic outcrop such as in the Goldfield area. An additional 1 degree, however, has to be added to the background limit of noise variation in the $\Delta \bar{R}_{\perp}$ direction. This will effect discrimination of weakly limonitic areas.

Because of the combined noise effects, the ferric iron targets must differ from background rock by 5 degrees or more in color space. In the LANDSAT data, the limonite spectral vectors normally vary up to 8 to 10 degrees from the background mean vector function with a continuous distribution of intermediate points. Given the

very tight discrimination parameters and he distribution of the data, it is obvious that conventionally used analysis techniques based on a statistical separation of the data into "clusters" will not be effective for the present application. It is also obvious that computerized techniques based on these very small spectral differences in the LANDSAT data, in order to be applied with reasonable confidence, require precise laboratory and field assessment of the spectral properties of the field targets and materials to be discriminated.

The low spectral contrast found in the present LANDSAT data can be improved with instrument modifications. The 15 percent reduction in spectral contrast due to the field of view phenomenon indicates the approximate increase to expect by reducing the sensor field of view on LANDSAT or high altitude aircraft from 80 meters to 20 meters while retaining the present spectral bands. Spectral contrast among the types of geologic targets in the survey area, however, can be increased much more by changing the spectral bands of the low resolution instrument. The ratio plots of optimum spectral bands (e.g. Figures 4 and 5) compared with the same ratio plots using simulated LANDSAT bands (Collins, 1976) show that a 100 percent increase in contrast can be achieved by changing the band configuration. This is an especially important design consideration in satellite applications where the discriminating signal is critically close to the atmospheric and geologic noise.

The more important effect of using a smaller field of view would be to reduce the ambiguity of discrimination due to material distribution, and to increase the resolution of spatial variations among ground targets. Alteration zones generally have a mottled pattern of ferric iron distribution while hematitic rock units or alluvium, which can be confused with iron enriched alteration zones, often have a more

homogeneous distribution of ferric iron minerals. A smaller field of view would enhance the pattern discriminability and help in separating altered zones from non-altered rock units or alluvium rich in hematite.

FIGURE CAPTIONS

Figure 1. Satellite 4 band spectral measurements in four dimensional hyperspace projected onto the two dimensional principal planes.

Figure 2. Geologic map of the Goldfield mining district adapted from the USGS open file map by Ashley (1971). The shaded area is the argillized zone of hydrothermal alteration adapted from Jensen, et al., (1971). Flight lines are plotted on the map from photographs taken simultaneously with the spectral data.

Figure 3. Measurements, in percent reflectance, of outcrop samples from the Goldfield area. Spectra were taken in the laboratory with the aircraft instrument and looking at the exposed, weathered surface of whole rock samples.

Figure 4. Flight line 24 ratio plots. The three combinations of ratios for the first three bands are plotted with respect to position along the flight line. The flight line is plotted on the geologic map (Figure 2). The letter symbols and boundaries correspond to rock units crossed by the flight path. Symbols are referenced below.

EXPLANATION OF ROCK SYMBOLS

Q	Quaternary alluvium and colluvium.	Td, Tdb	Miocene Goldfield Dacite.
Qp	Quaternary pediment gravels.	Tma	Miocene Milltown Andesite.
Tb	Pliocene basalt of Blackcap Mtn.	Tsf	Miocene Sandstorm Rhyolite.
Ts	Miocene Siebert Tuff.	Alt.	Hydrothermally altered rock.
Tls	Miocene Landslide Deposits.		

Figure 5. Flight line 2 ratio plots for the 6 combinations of all 4 bands.

Figure 6. Selected spectra from flight line 2 plotted in full wavelength resolution. The high frequency variations in the spectral curves are caused by gaseous absorption in the earth's atmosphere and groups of Fraunhofer absorption bands in the solar atmosphere.

Figure 7. Color space model for discriminating spectral variations in rock spectra due to ferric iron absorption.

Figure 8. Computer produced map of ferric iron rich areas in Goldfield and the 15 mile square surrounding region. Pixels indicating high ferric iron concentration have been outlined. The background is in grey scale.

REFERENCES

Albers, J. P., and Kleinhampl, F. J., 1970, Spatial relation of mineral deposits to Tertiary volcanic centers in Nevada: U.S. Geol. Survey Prof. Paper 700-C, p. C1-C10.

Ashley, R. P., 1971, Preliminary geologic map of the Goldfield mining district, Nevada: U.S. Geol. Survey open-file map.

Ashley, R. P., 1974, Goldfield mining district: Nevada Bureau of Mines and Geology Rept. 19, p. 49-66.

Chiu, Hong-Yee, and Collins, W., 1977, A spectroradiometer developed for airborne remote sensing applications: Photogrammetric Engineering and Remote Sensing (in press).

Collins, W., 1976, Spectroradiometric detection and mapping of areas enriched in ferric iron minerals using airborne and orbiting instruments, Ph. D. Dissertation, Columbia Univ.

Goetz, A. F. H., Billingsley, F. C., Gillespie, A. R., Abrams, M. J., Squires, R. L., Shoemaker, E. M., Lucchitta, I., and Elston, D. P., 1975, Application of ERTS images and image processing to regional geologic problems and geologic mapping in Northern Arizona: Jet Propulsion Laboratory Tech. Report 32-1597, 188 pp., Pasadena, Calif.

Hansen, J. E., 1969, Radiative transfer by doubling very thin layers: Astrophys. Journ., vol. 155, pp. 565-573.

Harvey, R. D., and Vitaliano, C. J., 1964, Wall-rock alteration in the Goldfield district, Nevada: Journ. Geol., vol. 72, pp. 564-579.

Hughes Aircraft Co., 1972, Multispectral Scanner System for ERTS Four Band Scanner System: NASA document NASA-CR-132758, 133 pp.

Hunt, G. R., and Salisbury, J. W., 1970, Visible and near-infrared spectra of minerals and rocks -- I. Silicate minerals: Modern Geology, vol. 1, pp. 283-300.

Hunt, G. R., and Salisbury, J. W., 1971, Visible and near-infrared spectra of minerals and rocks -- III. Oxides and hydroxides: Modern Geology, vol. 2, no. 3, pp. 195-205.

Instrumentation Specialties Company, Inc., nd., Instrumentation manual - model SRC spectroradiometer calibrator: Instrument Specialties Company, Inc., Lincoln, Neb.

Jensen, M. L., Ashley, R. P., and Albers, J. P., 1971, Primary and secondary sulfates at Goldfield, Nevada: Econ. Geol., vol. 66, pp. 618-626.

Kiang, R. K., and Collins, W. E., 1976, Linear atmospheric transform on LANDSAT Measurements [Abs.]: Purdue LARS Symposium Proceedings, June 29 - July 1, 1976, p. 2B-5.

Princeton Applied Research Corp. 1975, Optical multichannel analyzer (OMA), operating and service manual: Princeton Applied Research Corp., Princeton, New Jersey.

Rowan, L. C., Wetlaufer, P. H., Goetz, A. F. H., Billingsley, F. C., and Stewart, J. H., 1974, Discrimination of rock types and detection of hydrothermally altered areas in south-central Nevada by the use of computer-enhanced ERTS images: U.S. Geol. Survey Prof. Paper 883, 35 pp.

Rowan, L. C., Goetz, A. F. H., and Ashley, R. P., 1977, Discrimination of hydrothermally altered and unaltered rocks in visible and near-infrared multispectral images: Geophysics (in press).

Ungar, S. G., 1976, A color vector classification algorithm: unpublished.

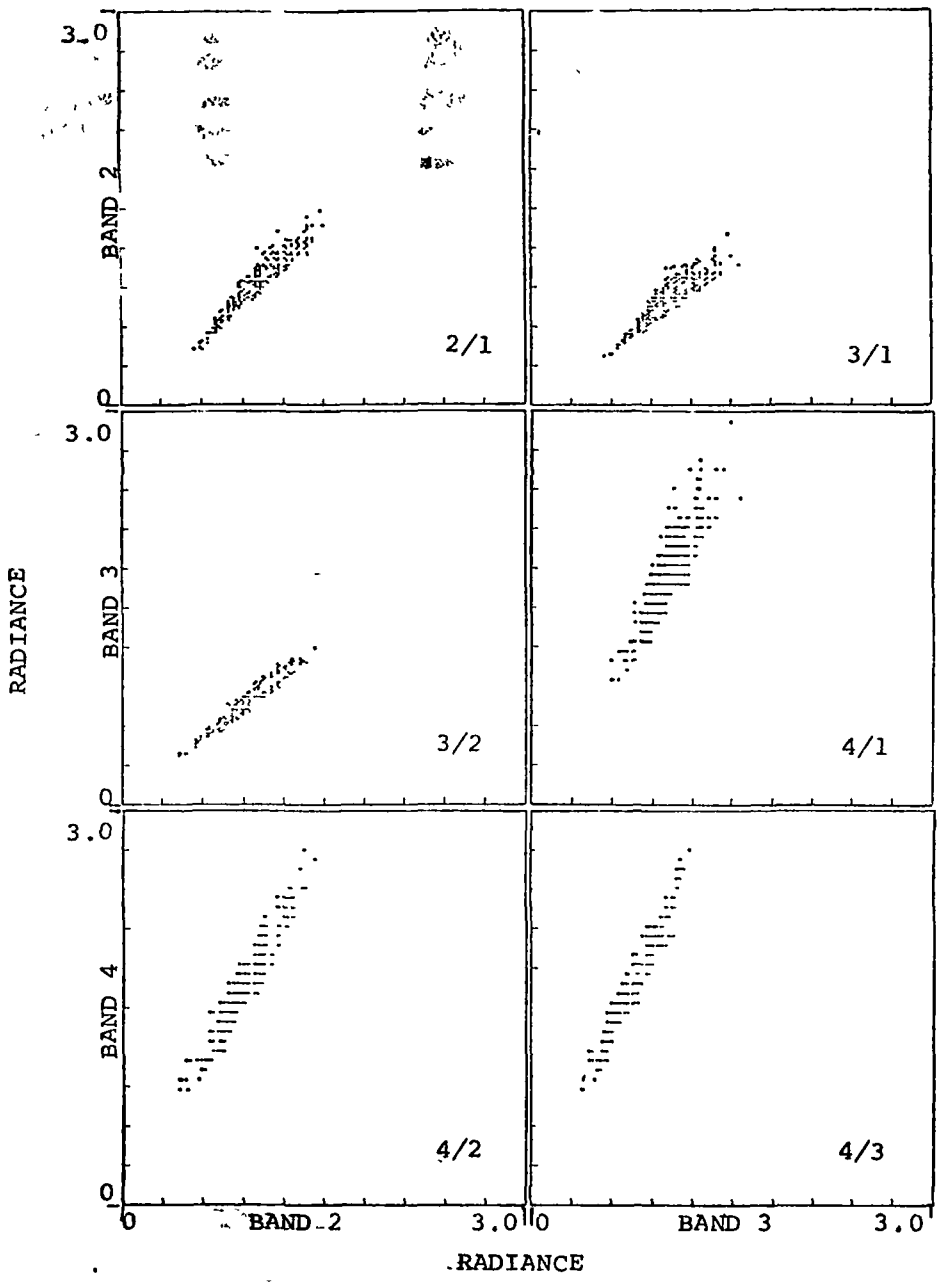
3.0
BAND 2
0
2/1
3/1
3.0
BAND 3
0
3/2
4/1
3.0
BAND 4
0
4/2
4/3
RADIANCE
0
BAND 2
3.0
0
BAND 3
3.0
RADIANCE

GEOLOGIC MAP OF THE GOLDFIELD MINING DISTRICT, NEVADA

ADAPTED FROM THE USGS OPEN FILE MAP BY R.P. ASHLEY

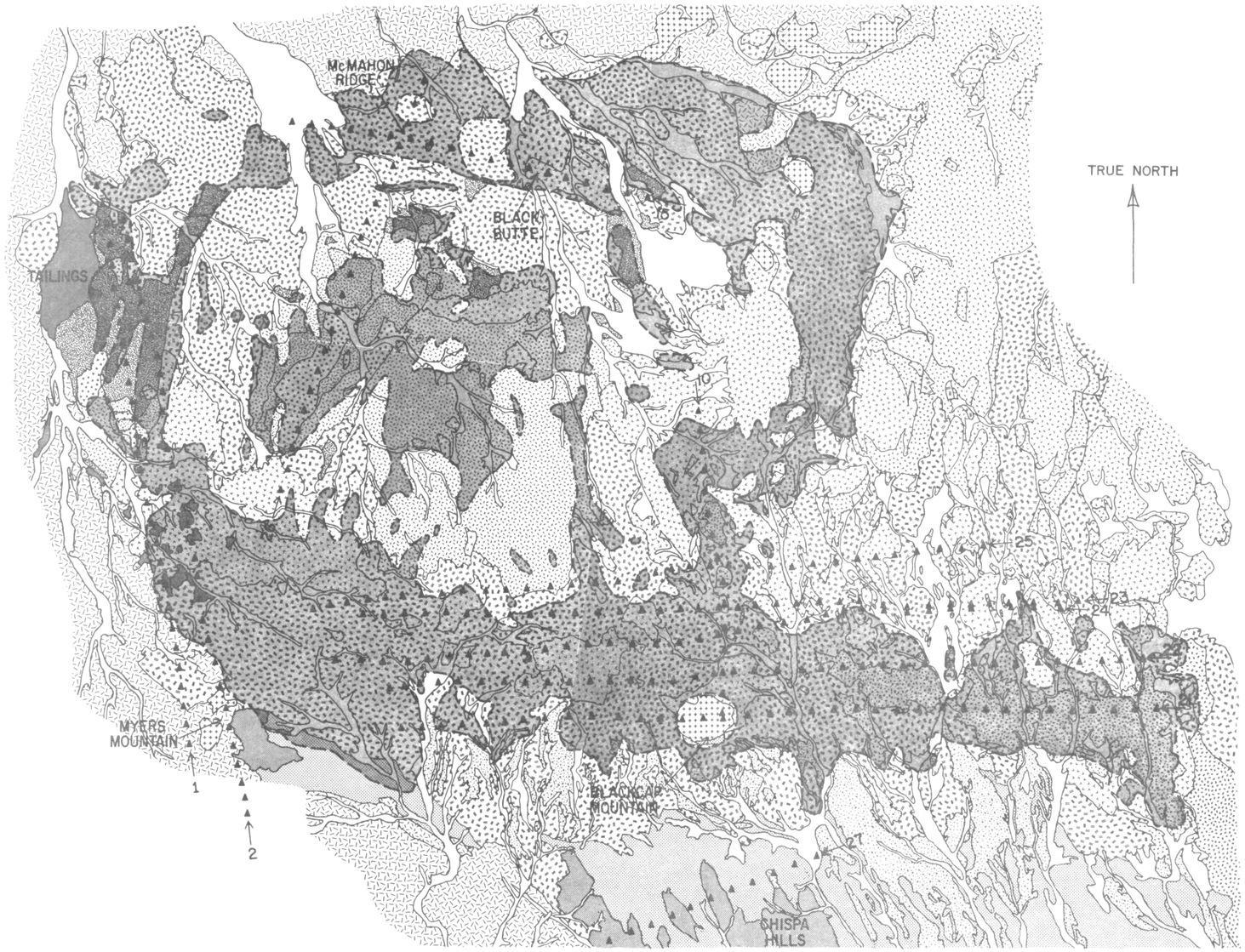

EXPLANATION

Quaternary

- Alluvium and Colluvium
- Pediment Gravels

Pliocene

- Malpais Basalt
- Spearhead Member Thirsty Canyon Tuff
- Basalt of Blackcap Mountain
- Siebert Formation
  Tuffaceous Sed. Rocks and Silicic Vitric Tuff
- Tuff of Meda Pass

Tertiary

Miocene

- Chispa Andesite
- Rhyolite of Wildhorse Spring

UNIFORMITY, HYDROTHERMAL ALTERATION AND ORE DEPOSITION

- Espina Breccia
- Dacite Vitrophyre
- Land Slide Deposits
- Goldfield Dacite
  Rhyodacite Flows / Vent Breccia
- Milltown Andesite
  Silicic Tuff and Ash-Flow Tuff
  Trachyandesite, Rhyodacite, and Quartz Latite Flows and Tuffs

Oligocene

- Sandstorm Rhyolite
  Rhyolite Flow and Ash-Flow Tuff
  Silicic Tuff, Lapilli Tuff
  and Tuff Breccia
- Goldfield Latite
  Quartz Latite Flow and Latitic Tuff
- Vindicator Rhyolite
  Rhyolite Flow and Silicic Ash-Flow Tuff

Jurassic

- Quartz Monzonite

- Contact
- Mine Dump, Tailings
- Approximate Limit of Argillized Zone
- Starting Point and Direction of Flight Line
- Every Tenth Spectral Measurement to Tape with Simultaneous Ground Truth Photograph

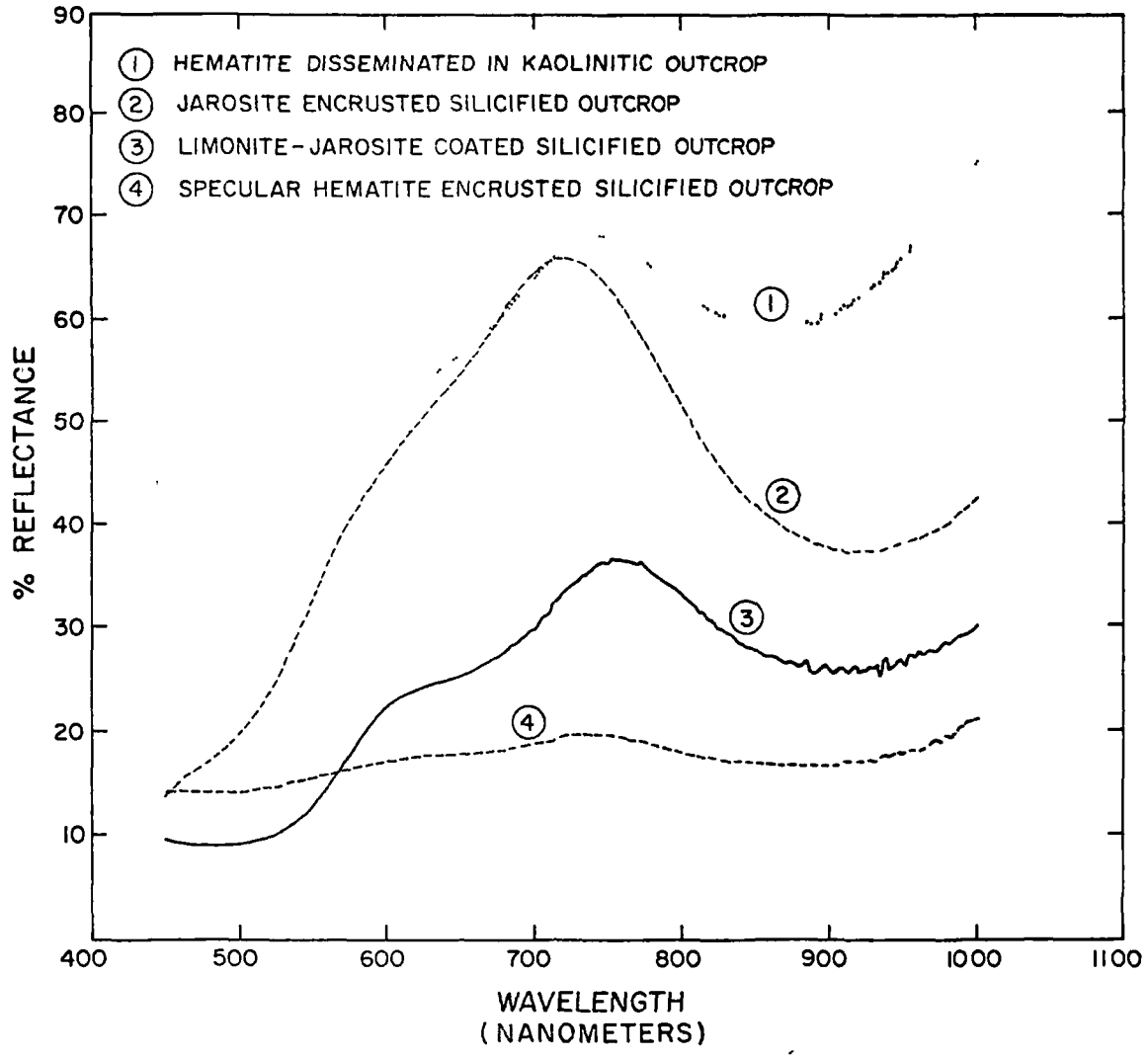
① HEMATITE DISSEMINATED IN KAOLINITIC OUTCROP
② JAROSITE ENCRUSTED SILICIFIED OUTCROP
③ LIMONITE-JAROSITE COATED SILICIFIED OUTCROP
④ SPECULAR HEMATITE ENCRUSTED SILICIFIED OUTCROP
% REFLECTANCE
90
80
70
60
50
40
30
20
10
400
500
600
700
800
900
1000
1100
WAVELENGTH
(NANOMETERS)

Fig 3

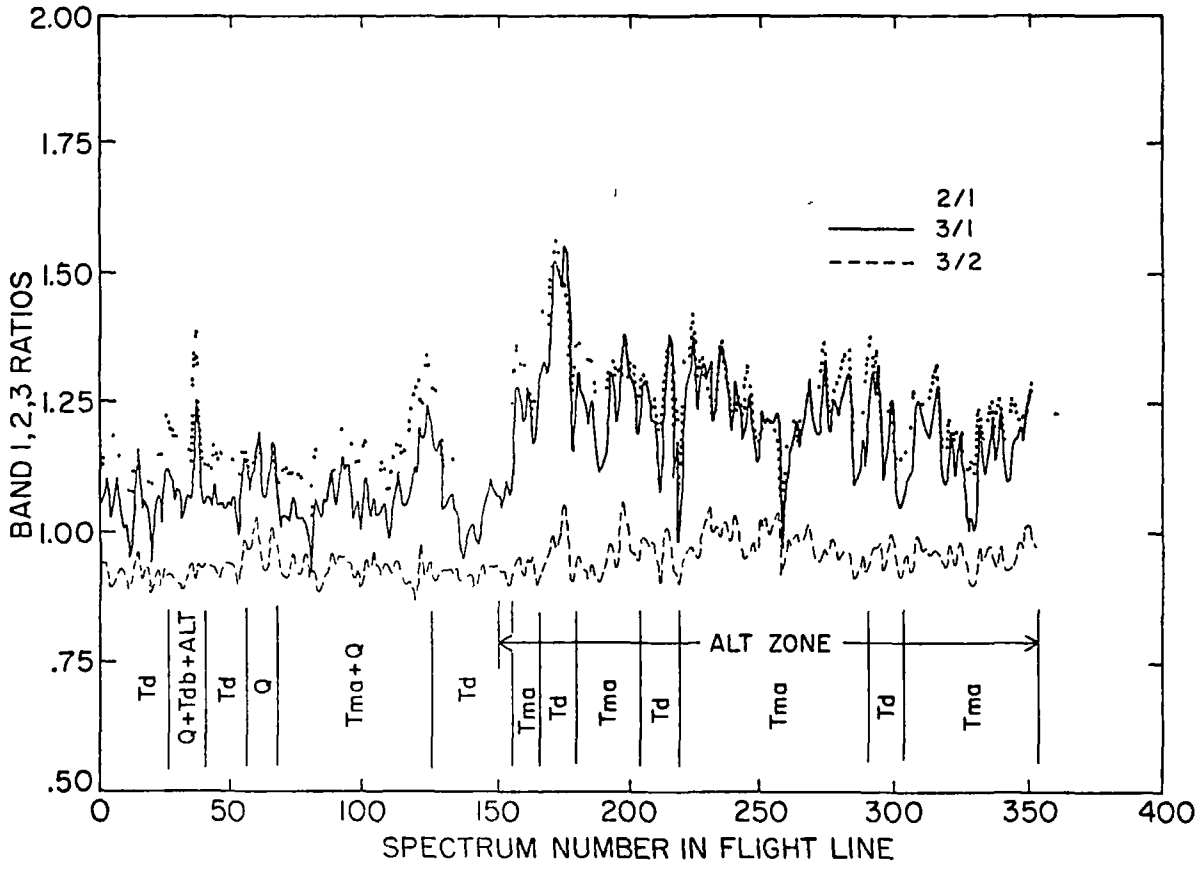
2.00
1.75
1.50
1.25
1.00
.75
.50
BAND 1,2,3 RATIOS
2/1
3/1
3/2
Td
Q+Tdb+ALT
Td
Q
Tma+Q
Td
Tma
Td
Tma
Td
ALT ZONE
Tma
Td
Tma
0
50
100
150
200
250
300
350
400
SPECTRUM NUMBER IN FLIGHT LINE

FIG 4

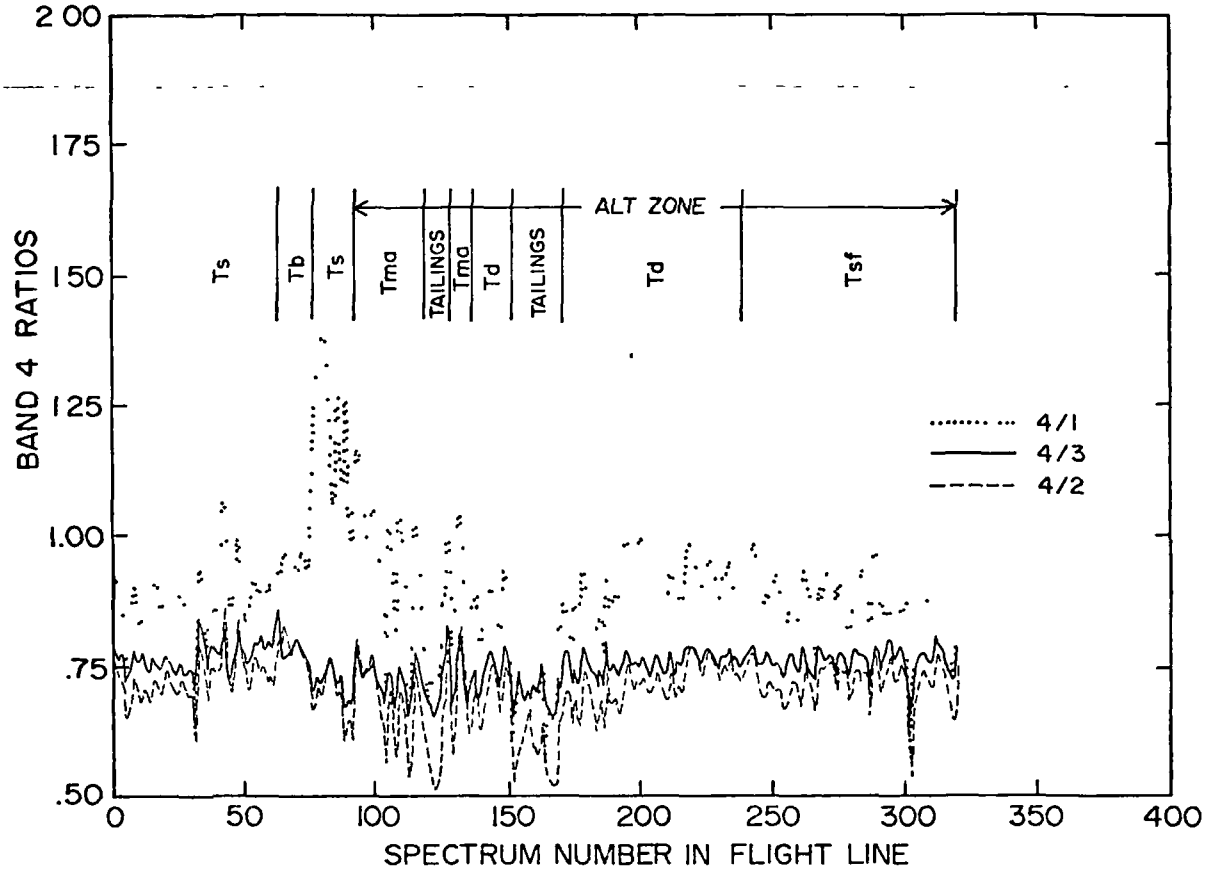
2.00
1.75
1.50
1.25
1.00
.75
.50
BAND 4 RATIOS
Ts
Tb
Ts
Tma
TAILINGS
Tma
Td
TAILINGS
ALT ZONE
Td
Tsf
4/1
4/3
4/2
0
50
100
150
200
250
300
350
400
SPECTRUM NUMBER IN FLIGHT LINE

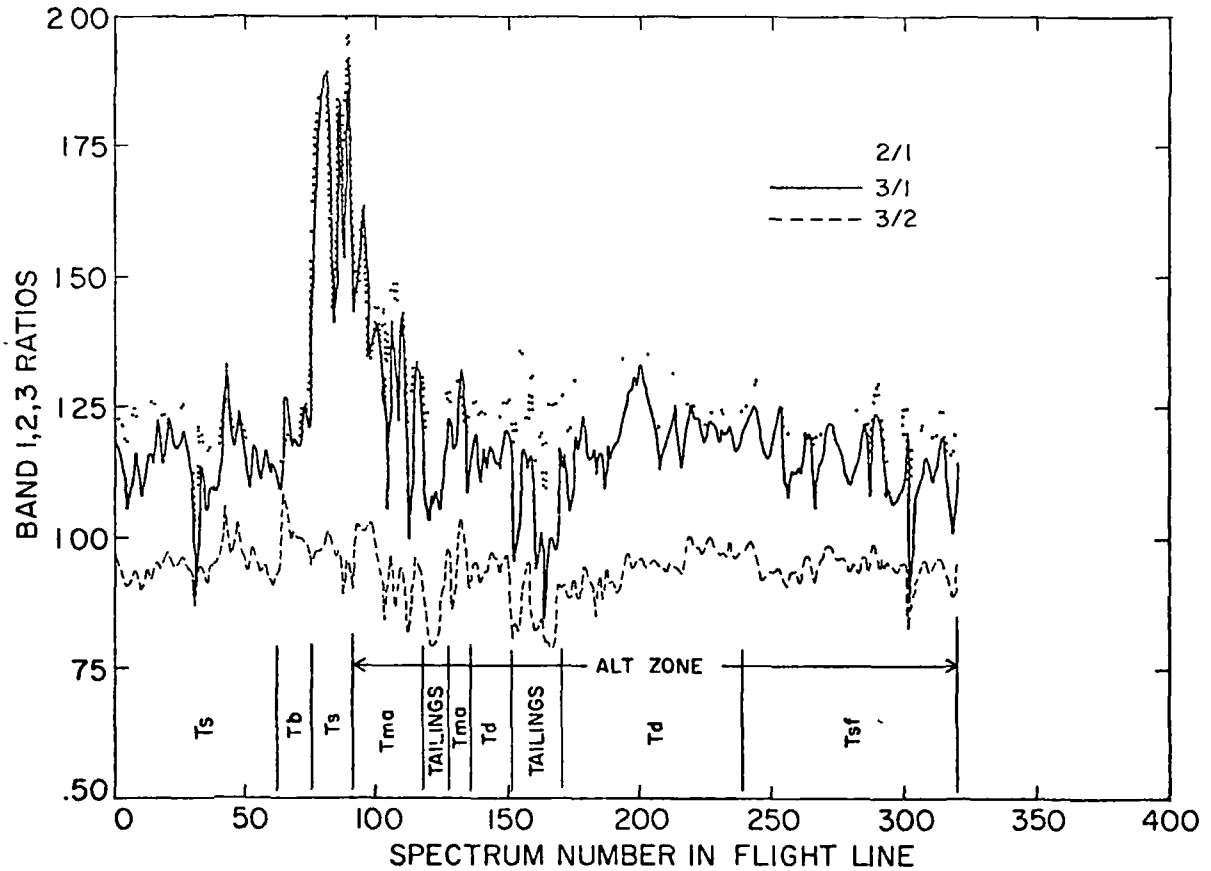
2.00
1.75
1.50
1.25
1.00
.75
.50
BAND 1,2,3 RATIOS
2/1
3/1
3/2
Ts
Tb
Ts
Tma
TAILINGS
Tma
Td
TAILINGS
ALT ZONE
Td
Tsf
0
50
100
150
200
250
300
350
400
SPECTRUM NUMBER IN FLIGHT LINE

FIG 5

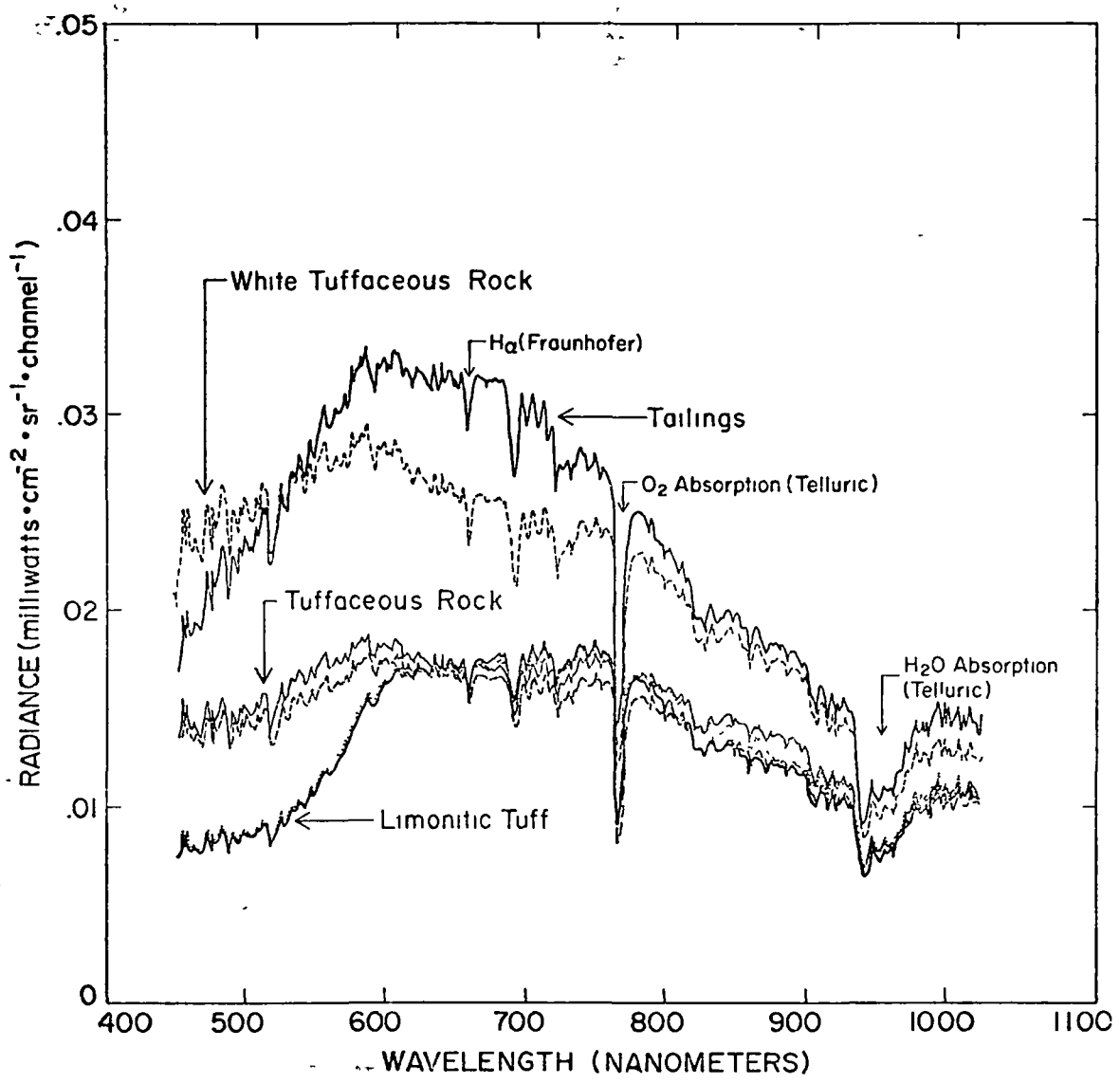
.05
.04
.03
.02
.01
0
RADIANCE (milliwatts • cm⁻² • sr⁻¹ • channel⁻¹)
White Tuffaceous Rock
Hα (Fraunhofer)
Tailings
O2 Absorption (Telluric)
Tuffaceous Rock
H2O Absorption (Telluric)
Limonitic Tuff
400
500
600
700
800
900
1000
1100
WAVELENGTH (NANOMETERS)

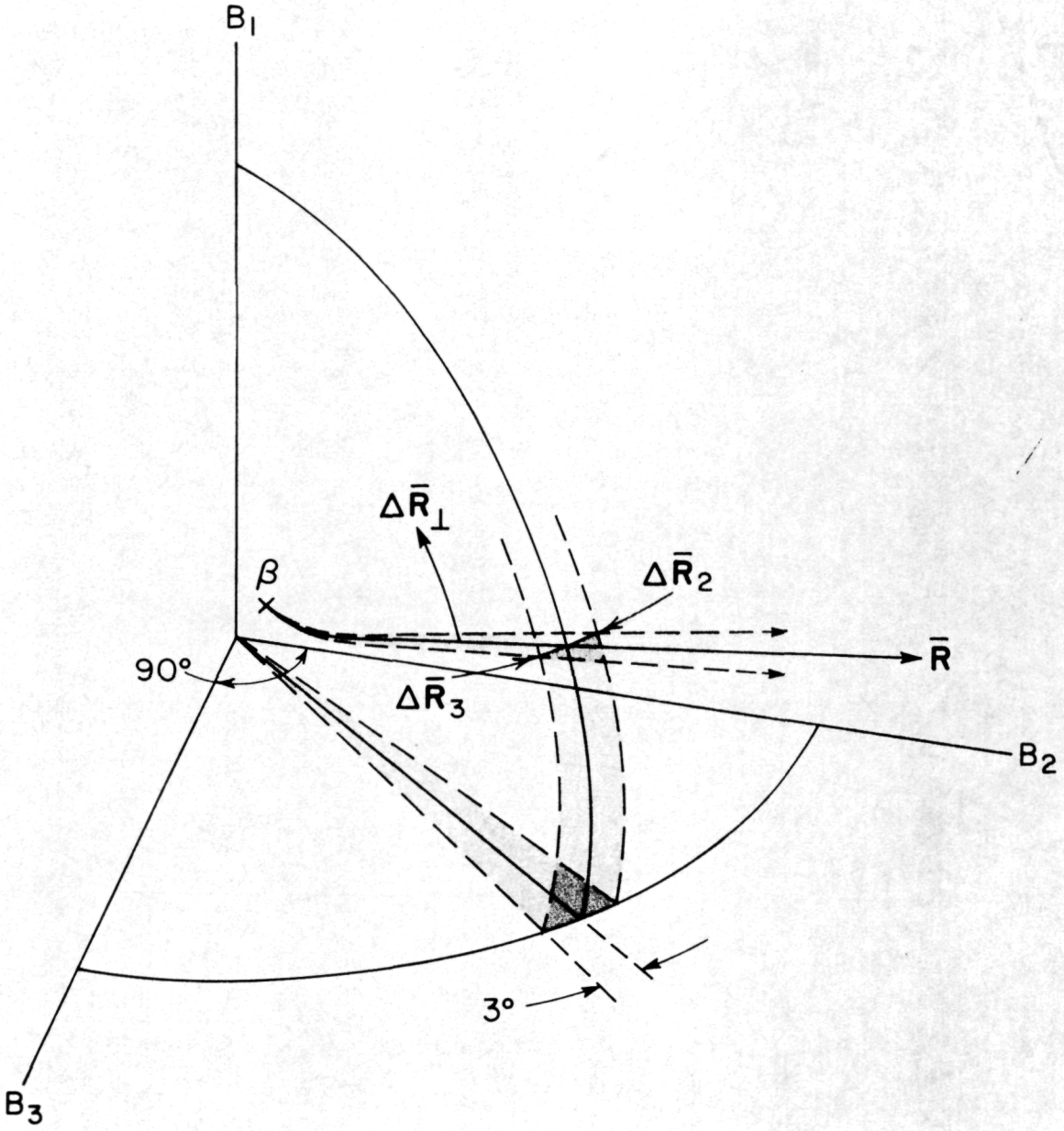
B1
ΔR⊥
β
ΔR2
R
90°
ΔR3
B2
3°
B3

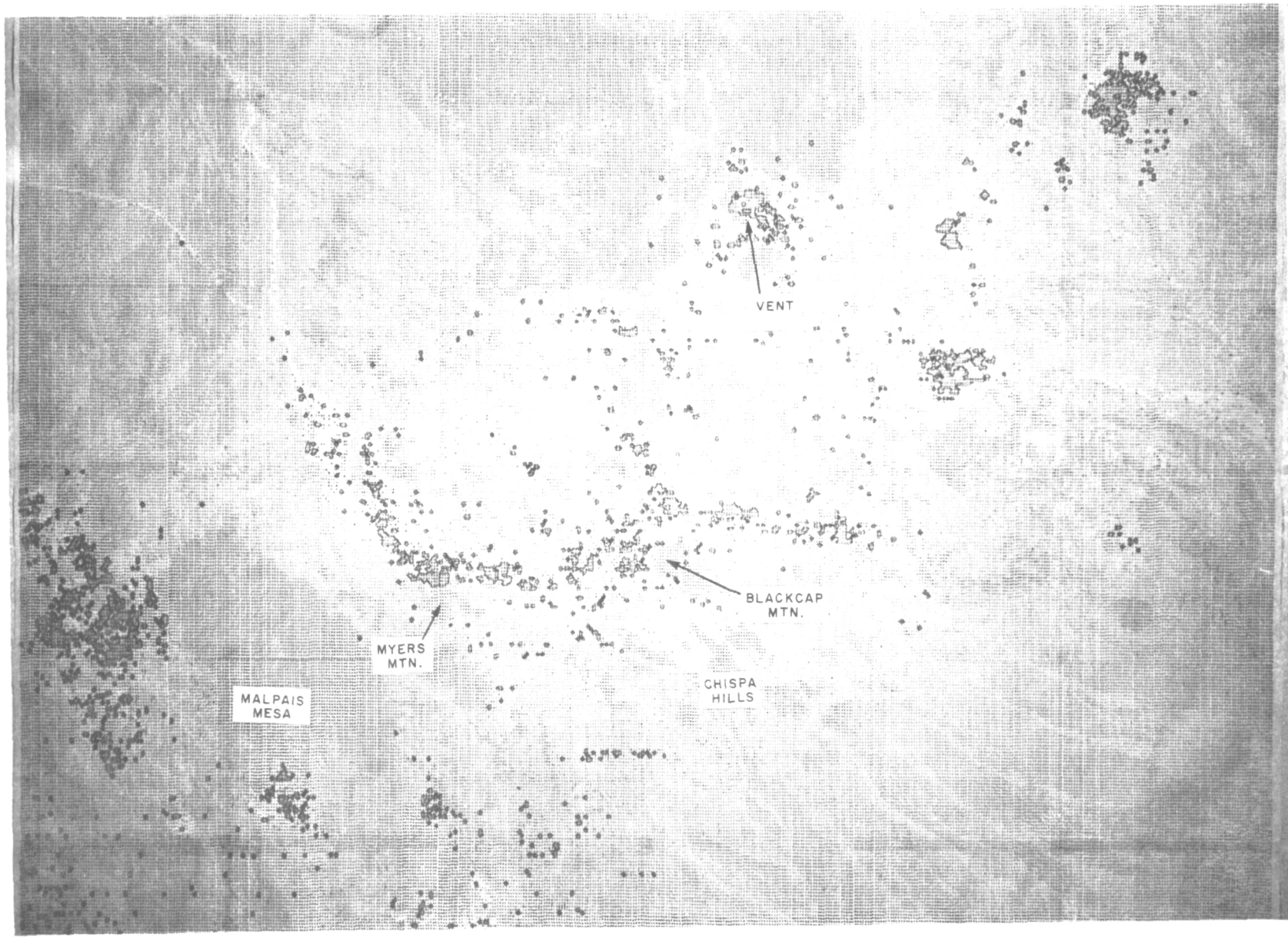
VENT
BLACKCAP MTN.
MYERS MTN.
CHISPA HILLS
MALPAIS MESA